*Materials Transactions*, Vol. 61, No. 3 (2020) pp. 506 to 514


# Effect of Cations on Protective Properties of Rust Layer Formed on Carbon Steel during Wet/Dry Cyclic Corrosion

Kyung-Tae Kim[1,*1], Hiroaki Tsuchiya[1], Koushu Hanaki[1,2], Masato Yamashita[1,2] and Shinji Fujimoto[1,*2]

[1]*Division of Materials and Manufacturing Science, Graduate School of Engineering, Osaka University, Suita 565-0871, Japan*
[2]*Kyoto Materials Co. Ltd., Kyoto 615-8245, Japan*

The present work proposed a simple approach to modify the morphology and composition of rust layers formed on carbon steel during wet/dry cyclic atmospheric corrosion, and thereby improve the protective properties of the rust layers. Rust layers were grown on carbon steel by a laboratory cyclic corrosion test. Additional immersion in sulfate solutions containing $Mg^{2+}$, $Al^{3+}$, $Cu^{2+}$, or $Ni^{2+}$ was carried out during the cyclic corrosion test to modify the rust layers. The morphology of the rust layers on carbon steel in the reference specimen that was not subjected to additional immersion showed a plate-like structure. The rust layers on the $Mg^{2+}$ specimen consisted of plate-like and needle structures. On the other hand, the other specimens subjected to additional immersion exhibited particulate structures, although the rust layers on the $Cu^{2+}$ specimen consisted of finer secondary particles. Rust layers on the $Al^{3+}$ specimen and the $Ni^{2+}$ specimen were denser compared to the other specimens. XRD revealed that the composition of the rust layer was changed by additional immersion, that is, on all the specimens subjected to the additional immersion, the growth of $\alpha$-FeOOH was enhanced whereas that of $Fe_3O_4$ was hindered. Variations in the corrosion potential and corrosion current density obtained from potentiodynamic polarization measurements were strongly related to the morphology and composition of the rust layers. [doi:10.2320/matertrans.MT-M2019270]

(Received September 20, 2019; Accepted December 25, 2019; Published February 25, 2020)

**Keywords:** *carbon steel, atmospheric corrosion, rust layer, cation, electrochemistry*

## 1. Introduction

Corrosion damage on steels considerably increases the maintenance cost of infrastructures. It is well-known that more than 3% of the world's GDP is expended due to corrosion.[1)] According to a recent U.S. corrosion survey, for example, the direct cost incurred for metallic corrosion was estimated as approximately $276 billion on an annual basis, which approximately constitutes 3.1% of the GDP.[2)] More than 50% of the corrosion cost is toward countermeasures against atmospheric corrosion.[3)]

Carbon steel is the most commonly employed metallic material for infrastructures due to its superior mechanical strength as well as low cost.[4)] As carbon steel is liable to corrode accompanying with the formation of rust in atmospheric environments, improvement in the corrosion resistance of carbon steel is required for prolonged usage of infrastructures. The rust layer on carbon steel in various atmospheric environments is known to consist of $\alpha$-FeOOH, $\beta$-FeOOH, $\gamma$-FeOOH, $Fe_3O_4$, and poorly crystallized iron oxides which are actually considered to be nano-sized crystals.[5)] The constituents of the rust layer are strongly related to the environment where the rust grows.[6)] For instance, $\alpha$-FeOOH and $\gamma$-FeOOH often form in urban and industrial regions, whereas $\beta$-FeOOH grows in $Cl^-$-containing environments such as sea shores.[4,7)] Furthermore, in environments with low oxygen activity, $Fe_3O_4$ becomes dominant in the rust layer. It is also well-known that characteristics of rust are different depending on the constituents. $\gamma$-FeOOH acts as an oxidizing agent which promotes corrosion. $\gamma$-FeOOH typically grows in the initial stage of atmospheric corrosion, but is unstable and transforms to $\alpha$-FeOOH during long-term exposure to the abovementioned environments. On the other hand, $\alpha$-FeOOH is recognized as the most stable phase among rusts and is also known to consist of smaller crystals than $\gamma$-FeOOH.[8)] Due to these characteristics, $\alpha$-FeOOH inhibits the penetration of corrosive species as well as water and oxygen through the rust to substrate steel. The presence of salinity in environment promotes the formation of $\beta$-FeOOH;[9)] however, this oxyhydroxide is also unstable and can be reduced relatively easily under wet/dry cyclic conditions. As the reduction of $\beta$-FeOOH is accompanied by the oxidation of substrate steel, corrosion is accelerated. Simultaneously, the reduction of $\beta$-FeOOH in wet/dry cycling results in the formation of $Fe_3O_4$. This type of iron oxide also accelerates the redox reaction in a wet rust layer due to its significantly higher electrical conductivity.[10)] Based on these discussions, $\alpha$-FeOOH is an important rust as a protective barrier against atmospheric corrosion on carbon steel. However, the formation of $\alpha$-FeOOH requires long-term exposure to the atmospheric environments as described above.

Weathering steels that contain small amounts of alloying elements such as Cu, Cr, Ni, P, Si and Mn have been widely used for infrastructures due to their improved atmospheric corrosion resistance compared to carbon steel. The superior atmospheric corrosion resistance is ascribed to a protective rust layer formed on weathering steels during long-term exposure to the atmosphere. Therefore, the rust layers formed on weathering steels were extensively characterized, and the structure and composition of the rust layers on the weathering steels were compared with those on mild and carbon steel.[11–16)] Yamashita *et al.* examined protective rust layers formed on weathering steels exposed for 17 years to air at various locations in Japan and found that the layers comprised mainly $\alpha$-FeOOH and some alloying elements such as Cr and Cu.[13)] Okada *et al.* also detected the enrichment of Cu and P in an inner layer of rust on a weathering steel and attributed the protectiveness of the steel to the enrichment of the elements.[14)] These imply that the introduction of these elements into the rust layer from the

*[1]Graduate Student, Osaka University
*[2]Corresponding author, E-mail: fujimoto@mat.eng.osaka-u.ac.jp

underlying substrate steel may modify the structure and composition of the rust and improve the resulting protectiveness of the rust layer. Although the addition of some elements such as Cr, Cu, Ni, and P to carbon steel was demonstrated to be effective in improving the atmospheric corrosion resistance, the amount of their addition would be limited due to possible detrimental effects to the mechanical properties, workability, and welding ability of carbon steel.

In the present work, we propose an alternative approach to modify the rust layer on carbon steel without the addition of the above-mentioned elements to the steel. Our approach is simple in that it involves the simple immersion of carbon steel into solutions that contain cations of such elements. Furthermore, effects of the cations on the structure and protective property of the rust layer formed on a carbon steel are discussed.

## 2. Experimental Procedure

### 2.1 Material preparation

The materials examined were carbon steel (SS400-JIS G3101) sheets, the chemical composition of which is provided in Table 1. Specimens of size of $20 \times 27 \times 3\,mm^3$ were cut from the sheets. After polishing the specimen surfaces with SiC abrasive papers up to #600, they were rinsed in methanol and then dried in air.

### 2.2 Wet/dry cyclic corrosion test

A laboratory cyclic corrosion test was performed for the polished specimens according to SAE J2334.[17] The SAE J2334 simulates a severe atmospheric corrosion environment and has been often used to evaluate the atmospheric corrosion resistance of steels.[18,19] In the SAE J2334 test, the polished specimens were kept for 6 h in a tightly sealed box where the temperature and relative humidity (R. H.) were controlled at 50°C and 100%, respectively (humid stage). Subsequently, the specimens were immersed in an aqueous solution containing 0.5 mass% NaCl, 0.1 mass% $CaCl_2$, and 0.075 mass% $NaHCO_3$ for 15 min. (immersion stage), followed by holding for 17 h 45 min. in the box at 60°C and 50% R. H. (dry stage). These three steps were repeated up to 50 cycles. As schematically explained in Fig. 1, the specimens were immersed in a solution of 1 M $MgSO_4$, $Al_2(SO_4)_3$, $CuSO_4$, or $NiSO_4$ for 5 s prior to the humid stage at each cycle from the 2nd cycle. These specimens are hereinafter referred to as $Mg^{2+}$, $Al^{3+}$, $Cu^{2+}$, or $Ni^{2+}$ specimens, respectively. Some specimens were not subjected to this process for reference (referred to as "reference specimen").

### 2.3 Characterization of rust layer

The morphology of the rusts formed on the specimens during the cyclic corrosion test was observed by scanning electron microscopy (SEM, JEOL JSM-5600) with an accelerating voltage of 25 kV. In order to identify the phase of the rusts, X-ray diffraction (XRD) measurements were carried out in the $2\theta$ angle range of 10° to 80° with a scan speed of $0.5°\,min.^{-1}$ using a Phillips X'pert Pro X-ray diffractometer, with a Cu target operated at 45 kV and 40 mA.

### 2.4 Electrochemical measurements

Potentiodynamic polarization of the rusts formed on the specimens during the cyclic corrosion test was carried out with a scan rate of $1\,mV\,s^{-1}$ at room temperature in a conventional three-electrode cell with a platinum counter electrode and a Ag/AgCl reference electrode in order to evaluate the electrochemical properties of the rusts. The polarization measurements commenced in the aqueous solution containing 0.5 mass% NaCl, 0.1 mass% $CaCl_2$, and 0.075 mass% $NaHCO_3$ without deaeration after a simple immersion of the specimens for 60 min.

Table 1 Chemical composition of the steel examined.

(mass%)

| C | Si | Mn | P | S | Fe |
|---|---|---|---|---|---|
| 0.05 | 0.03 | 0.33 | 0.016 | 0.01 | bal. |

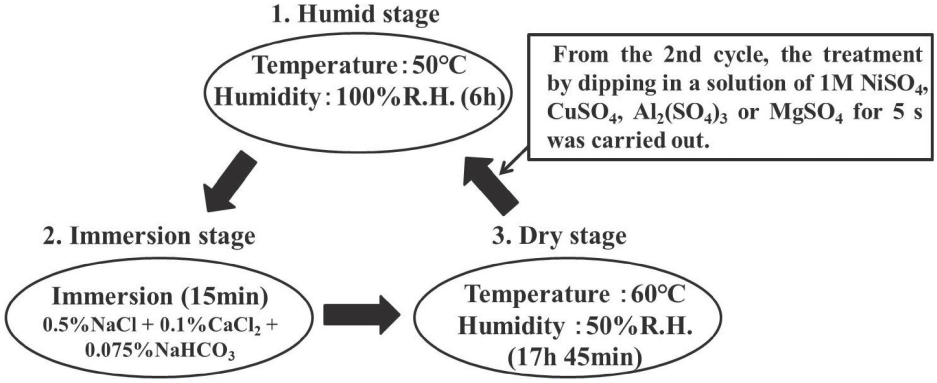


Fig. 1 Schematic diagram illustrating the laboratory cyclic corrosion test in wet/dry condition.

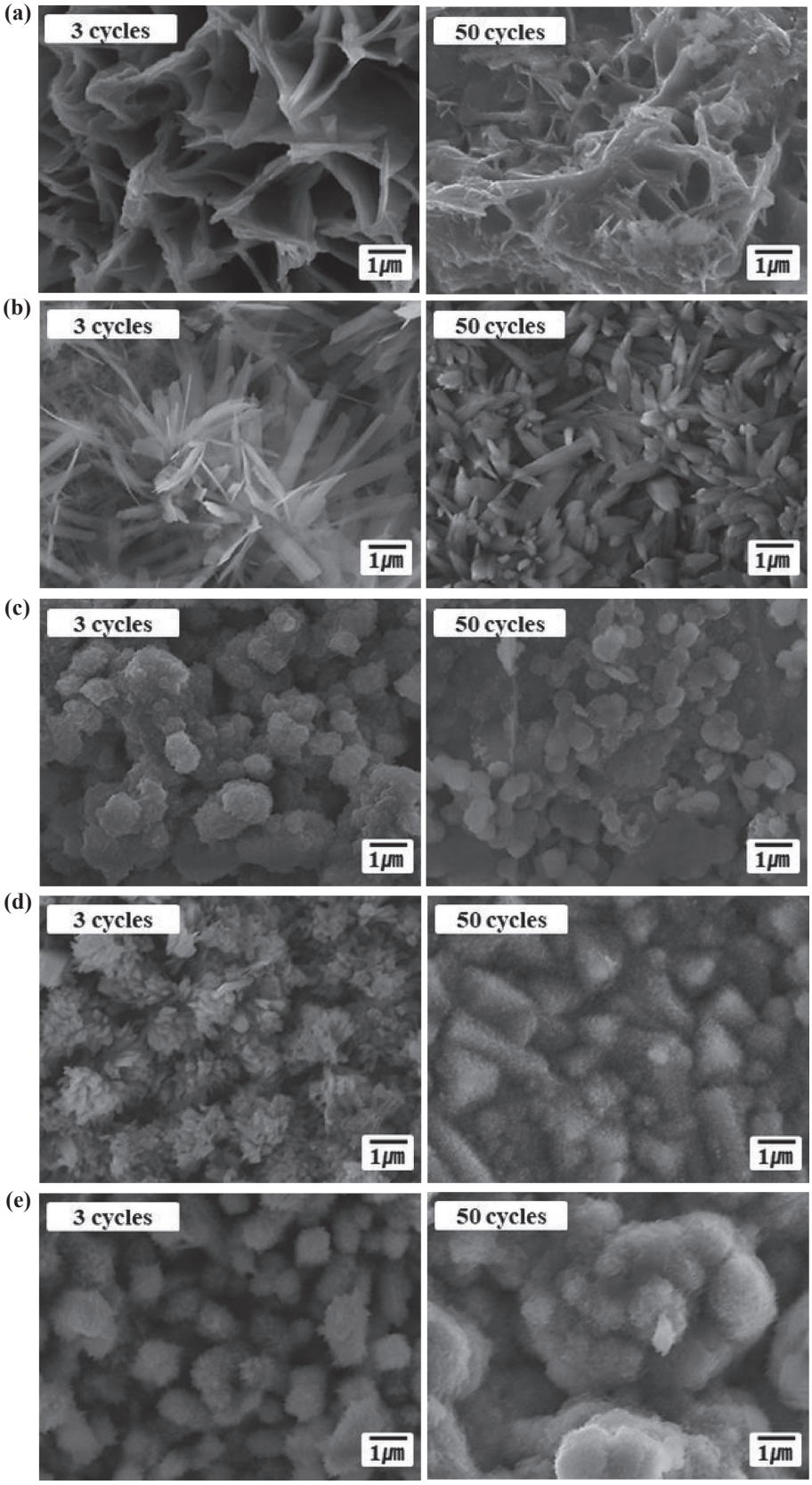


Fig. 2 SEM images of surfaces of rust layers on the carbon steel after 3 and 50 cycles of the atmospheric corrosion test; (a) reference, (b) $Mg^{2+}$, (c) $Al^{3+}$, (d) $Cu^{2+}$, and (e) $Ni^{2+}$.

## 3. Results

### 3.1 Morphology of rust layer

Figure 2 shows the top-view SEM images of each specimen after 3 and 50 cycles of the cyclic corrosion test. Growth of the rust layers is evident on all the specimens, only after 3 cycles of the cyclic corrosion test. However, the morphologies of the rust layers are different, depending on

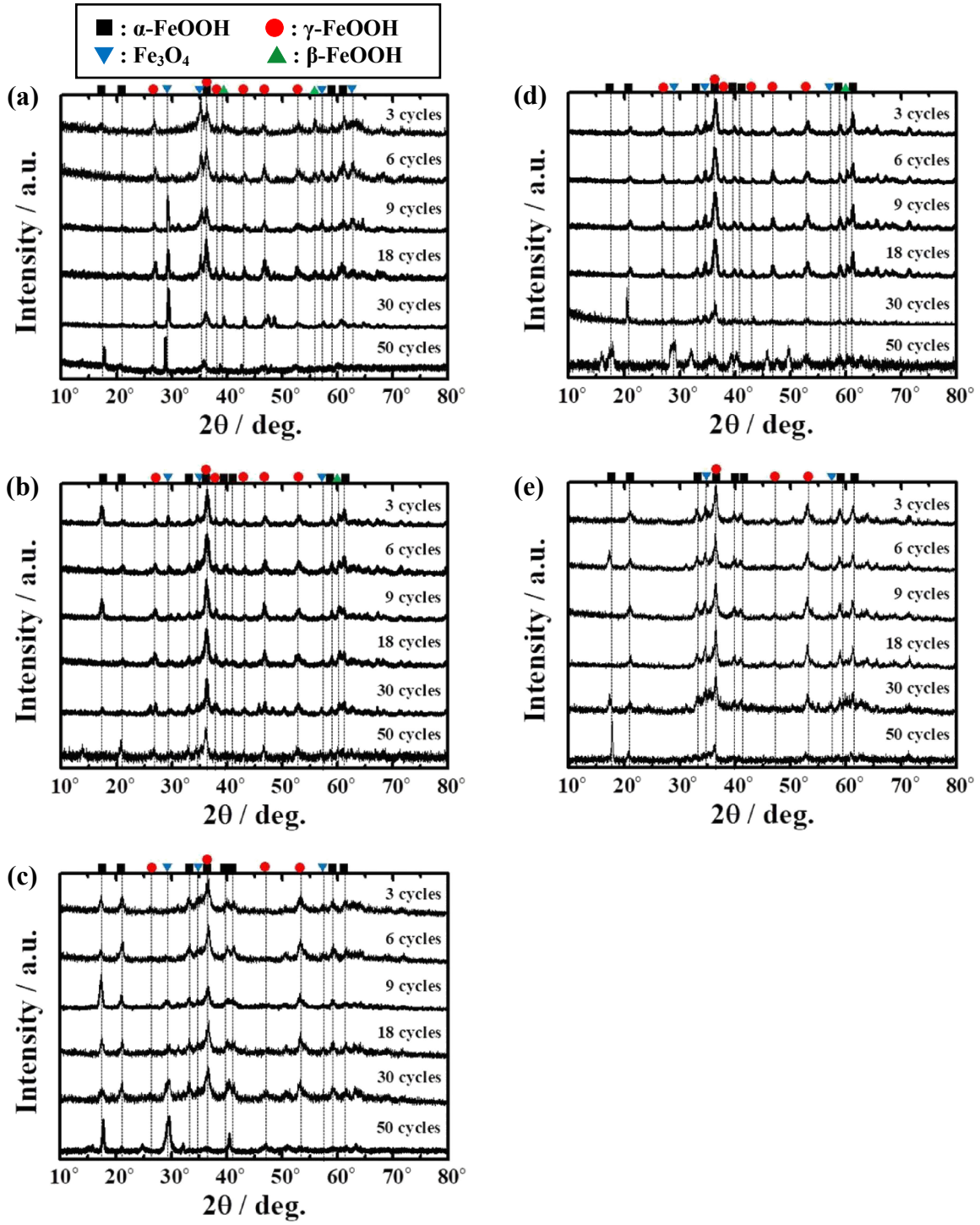


Fig. 3 X-ray diffraction patterns obtained from the specimens that were subjected to the atmospheric corrosion test; (a) reference, (b) $Mg^{2+}$, (c) $Al^{3+}$, (d) $Cu^{2+}$, and (e) $Ni^{2+}$.

the specimens. The rust layers on the reference specimen exhibited a plate-like structure in all cycles examined whereas those on the $Mg^{2+}$ specimen exhibit plate-like and needle structures. The rust layers on both specimens are not compact, but exhibit many hollows. On the other hand, rust layers with less hollows are observed to have grown on the other specimens, that is, on the $Cu^{2+}$, $Al^{3+}$ and $Ni^{2+}$ specimens. The rust layers on these three specimens show particulate structure, although the rust particles observed on the $Cu^{2+}$ specimen are composed of fine secondary particles. The compactness of the rust layers on all specimens is observed to improve with cycling.

### 3.2 Phase identification of rust layers

Figure 3 presents the XRD patterns for the specimens after certain cycles of the corrosion tests (3, 6, 9, 18, 30 and 50 cycles). Diffraction peaks assigned to $\alpha$-FeOOH, $\gamma$-FeOOH, and $Fe_3O_4$ are clearly observed for all the specimens whereas small peaks from $\beta$-FeOOH are recognized on the reference, $Mg^{2+}$, $Cu^{2+}$ specimens. This indicates that the rust layers

formed on the carbon steel during the cyclic corrosion test comprise the iron oxide and the oxyhydroxides. However, considering peak intensity of each constituent, the fractions of the oxide and oxyhydroxides in the rust layers are different depending on the experimental conditions. Therefore, the mass fractions of $\alpha$-FeOOH, $\beta$-FeOOH, $\gamma$-FeOOH, and $Fe_3O_4$ ($M_\alpha$, $M_\beta$, $M_\gamma$, and $M_S$, respectively) in the rust layers were calculated in order to evaluate the rust layers quantitatively using the intensity of the diffraction peaks obtained for each crystalline phase ($I_\alpha$, $I_\beta$, $I_\gamma$, and $I_S$, respectively) based on the following equation,

$$M_i = M_{iA} \cdot (I_i/I_{iA}) \Big/ \sum (M_{jA} \cdot I_j/I_{jA}) \quad (i, j = \alpha, \beta, \gamma, S) \tag{1}$$

where $I_{iA}$, $I_{jA}$ and $M_{iA}$, $M_{jA}$ are the reference diffraction intensities and the reference mass fractions obtained from the reference rust used in our previous work. Details on the estimation are described in the literature.[20)]

Figure 4 summarizes the calculated mass fractions of the rust phases formed on each specimen recognized in Fig. 3. The figures indicate that the rust composition also depends on the specimens. On the reference specimen, either $\gamma$-FeOOH or $Fe_3O_4$ is the main phase in the rust layers, whereas on the other specimens subjected to the additional immersion in the cation-containing solutions, $\alpha$-FeOOH is dominant. In particular, on the $Al^{3+}$ specimen and the $Ni^{2+}$ specimen, approximately 70% of the rust layers is $\alpha$-FeOOH. On the other hand, the $\alpha$-FeOOH in the rust layers grown on the $Mg^{2+}$ specimen and the $Cu^{2+}$ specimen is limited to approximately 50%. The rests of the rust layers are composed of $\beta$-FeOOH, $\gamma$-FeOOH, and $Fe_3O_4$ on the $Mg^{2+}$ specimen and the $Cu^{2+}$ specimen whereas no trace of $\beta$-FeOOH is detected as the other phases than $\alpha$-FeOOH in the rust layers formed on the $Al^{3+}$ and the $Ni^{2+}$ specimens. Therefore, the composition of the rust layer on carbon steel is modified by the additional immersion into the cation-containing solutions in the cyclic corrosion test, that is, by the introduction of cations into the rust layers.

### 3.3 Crystallite size of rusts

In addition to the phase identification of the rust layers described above, in the present work, the crystallite size of the main constituent of rust layers was evaluated based on Scherrer's equation,

$$D = \frac{0.9\lambda}{\beta \cos\theta} \tag{2}$$

where $D$ is the crystallite size, $\lambda$ is the wavelength of the incident X-ray (1.54 Å for CuK$\alpha$), $\beta$ is the full width at half maximum of the diffraction peak in radians, and $\theta$ is the Bragg angle of the peak. Either $\gamma$-FeOOH or $Fe_3O_4$ is the main constituent for the reference specimen depending on the number of cycles whereas $\alpha$-FeOOH accounts for a major portion of rust layer for the other specimens, independent of the cycles, as shown in Fig. 4. Figure 5 exhibits the crystallite sizes estimated for the main constituent in the rust layers. The crystallite size obtained for the reference specimen increases with the cycle number, whereas the sizes for the other specimens are smaller and remain almost constant.

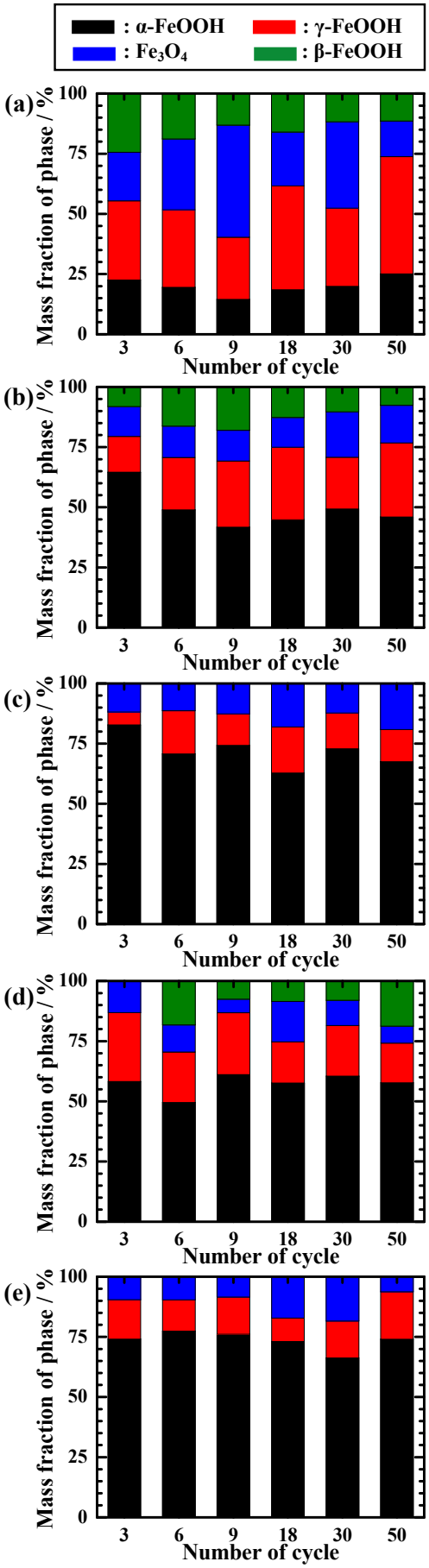


Fig. 4 Mass fractions of each constituent of the rusts obtained from the specimens that were subjected to the atmospheric corrosion test; (a) reference, (b) $Mg^{2+}$, (c) $Al^{3+}$, (d) $Cu^{2+}$, and (e) $Ni^{2+}$.

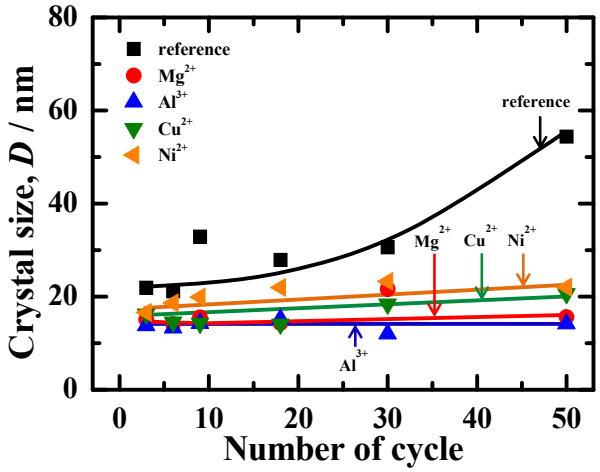


Fig. 5 Crystal size of a main constituent of rust layer on specimens with number of cycles.

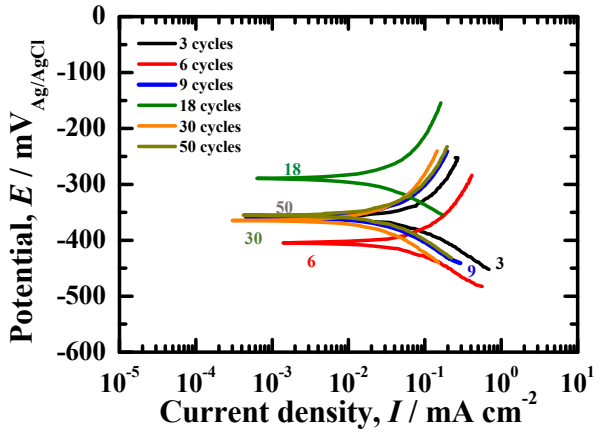


Fig. 6 Polarization curves of reference specimens after the cyclic corrosion test.

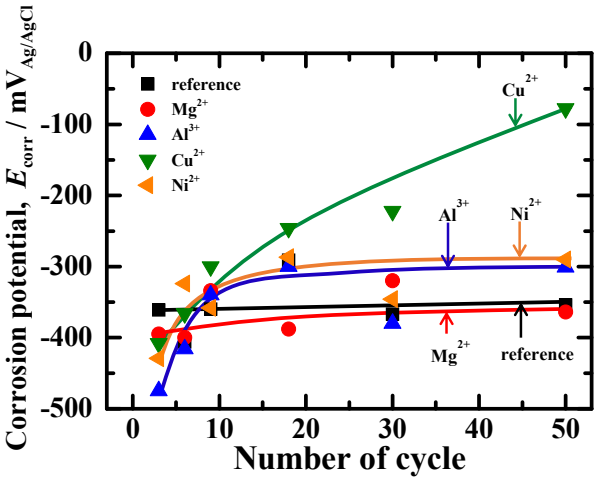


Fig. 7 Corrosion potential of specimens with number of cycles.

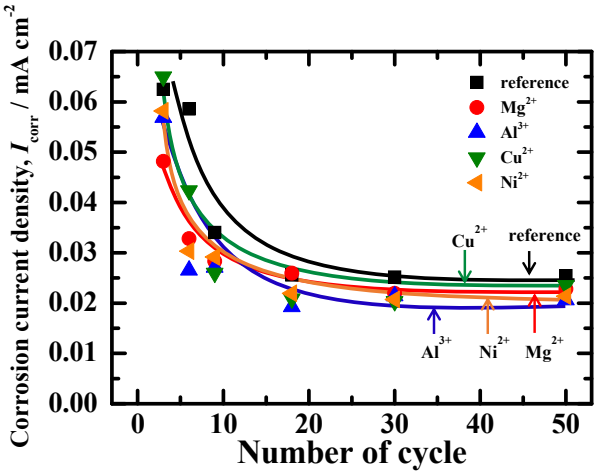


Fig. 8 Corrosion current density of specimens with number of cycles.

### 3.4 Electrochemical behavior of rust layers

Figure 6 shows representative polarization curves obtained for the reference specimens after the cyclic corrosion test. As explained above, the curves were measured in the aqueous solution containing 0.5 mass% NaCl, 0.1 mass% $CaCl_2$, and 0.075 mass% $NaHCO_3$, which is the same solution as that used in the immersion stage of the cyclic corrosion test. The corrosion potential, $E_{corr}$, and corrosion current density, $I_{corr}$, were estimated by extrapolation of the Tafel slopes within the potential range of ±100 mV from $E_{corr}$ in the polarization curve. $E_{corr}$ and $I_{corr}$ estimated from the polarization curves for all the rust layers are summarized with respect to the cycle of the corrosion test in Figs. 7 and 8, respectively. $E_{corr}$ clearly shifts in the noble direction for all the specimens with the cycle number although the variations of $E_{corr}$ are largely different, depending on specimen. $E_{corr}$ of the reference and the $Mg^{2+}$ specimens slightly increases. On the other hand, $E_{corr}$ of the $Al^{3+}$ and the $Ni^{2+}$ specimens drastically increases in the early stage and then levels off after 18th cycle. Furthermore, $E_{corr}$ of the $Cu^{2+}$ specimen tends to continuously increase with cycling and is obviously higher than those for the other specimens. On the other hand, $I_{corr}$ gradually decreases with the cycle number for all conditions. The reference specimen shows a slightly higher $I_{corr}$ compared to the other specimens. Therefore, even the electrochemical behavior of the rust layer formed on carbon steel is modified by the additional immersion in the cation containing solutions.

## 4. Discussions

### 4.1 Correlation between corrosion potential and corrosion current density

In Figs. 7 and 8, $E_{corr}$ and $I_{corr}$ are presented with respect to the number of cycles in the cyclic corrosion test. In Fig. 9, these variables are plotted in a graph to determine their correlation. The growth process of rust layers on all specimens can be divided in two stages: the initial stage up to the 3rd cycle and the second stage from the 6th cycle.

As mentioned above, the rust layer on the reference specimen was not compact during the initial stage of the cyclic corrosion test. The loose and porous rust layers were supposed not to inhibit the penetration of water, oxygen and corrosive ions which induce corrosion. Therefore, $I_{corr}$ was large and did not decrease so much in the initial stage, compared to the other specimens as shown in Fig. 9(a). However, in the second stage, $I_{corr}$ relatively decreased with increasing cycles in the corrosion test, and was accompanied

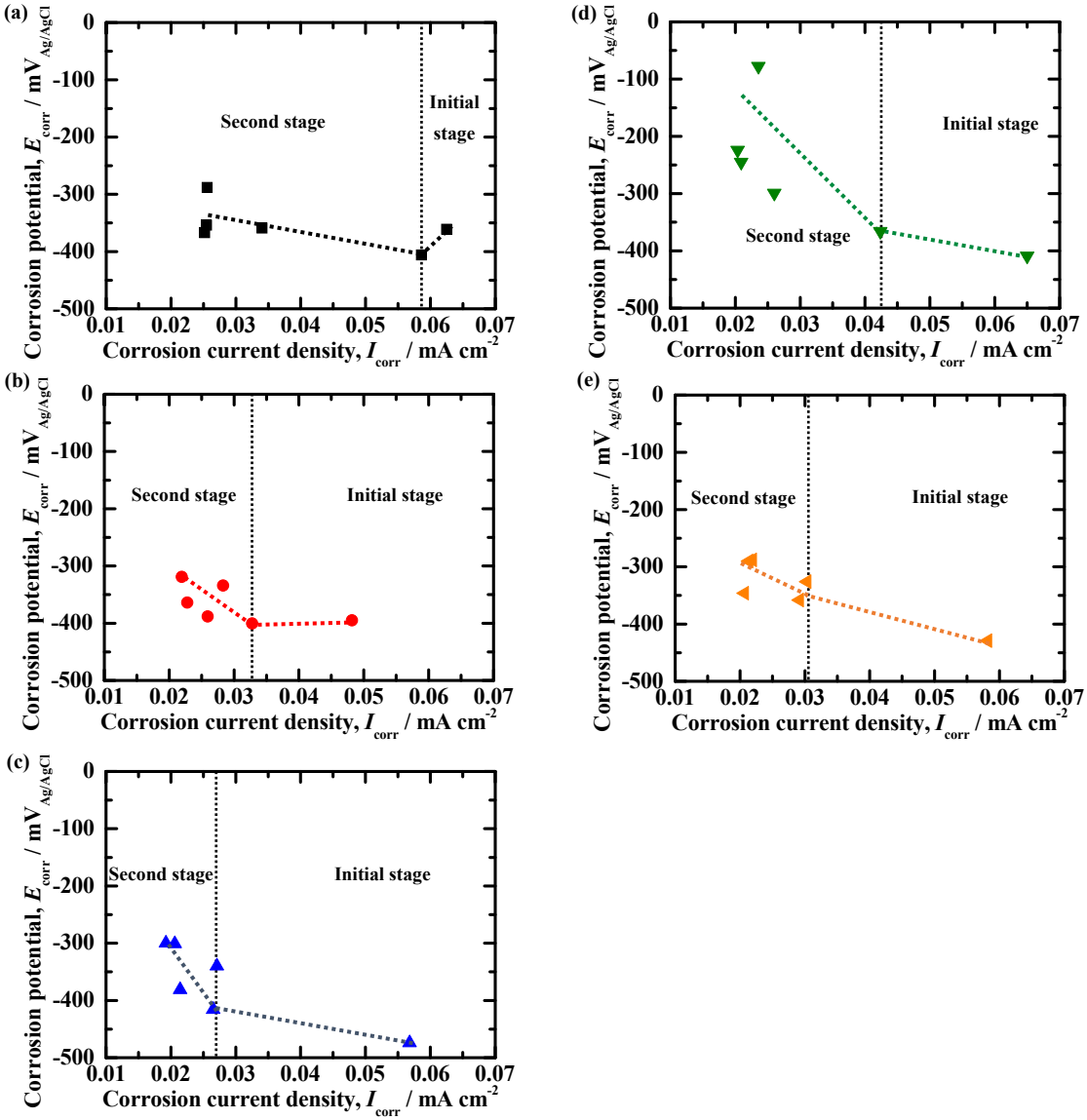


Fig. 9 Relation between corrosion potential and corrosion current density; (a) reference, (b) $Mg^{2+}$, (c) $Al^{3+}$, (d) $Cu^{2+}$, and (e) $Ni^{2+}$.

by a slight increase in $E_{corr}$. According to Chen *et al.*,[21] during the initial stage of atmospheric corrosion of steels, a sufficient supply of oxygen and corrosive ions through the porous rust layer enhanced corrosion as the porous layer did not act as a protective barrier to further corrosion. However, with the growth of the rust layer, that is, with increasing the layer thickness, the supply to the interface between the rust and the underlying substrate steel was suppressed due to the improved barrier effect of the rust layer.[22] In general, corrosive ions contributes to anodic reaction while oxygen contributes to cathodic reaction in corrosion under atmospheric corrosion. Therefore, based on the variations in $E_{corr}$ and $I_{corr}$ during the cycle of the corrosion test and the abovementioned discussions, the improved compactness of the rust layer was found to suppress anodic and cathodic reactions.

In the followings, the effects of cations on $E_{corr}$ and $I_{corr}$ in the initial stage and the second stage are discussed. In the initial stage, a drastic decrease of $I_{corr}$ was observed in the specimens that were subjected to the additional immersion in the cation containing solutions, especially the $Al^{3+}$ and the $Ni^{2+}$ specimens. Effects of cations on the growth of rust were already reported in the literature where weathering steels were examined. Mizoguchi *et al.* and Kimura *et al.* noted that alloying Ni and Cu in weathering steels contributed to the formation of rust layers composed of densely packed fine particles that suppressed the crystal growth of rust particles.[23,24] Hao *et al.* and Chen *et al.* also reported that Cu retarded the growth of rust grains, resulting in the growth of fine and dense rust layers that suppressed the supply of oxygen to the steel surface.[3,25,26] In addition, Cu was reported to suppress the crystallization of rust and contribute to form a crack-free rust layer.[27,28] On the other hand, Nishimura *et al.* found that Ni promoted the densification and refinement of rust.[29] Moreover, it was reported that Ni inhibited the growth of fine nuclei to large crystallines, yielding a protective rust layer with a fine and compact morphology.[30] Although effects of $Al^{3+}$ and $Mg^{2+}$ on the mechanism of densification and refinement of rust are not clear at the moment, based on the discussions mentioned above and the similarity of the correlation between $E_{corr}$ and $I_{corr}$ presented in Fig. 9, not only $Ni^{2+}$ and $Cu^{2+}$ but also $Al^{3+}$

and $Mg^{2+}$ are supposed to promote the densification and refinement of rust, which resulted in the decrease in $I_{corr}$. As shown in Fig. 2, the densification of the rust layer was apparently promoted on $Al^{3+}$ and $Ni^{2+}$ specimens, where a more drastic decrease in $I_{corr}$ was observed. Therefore, the morphology of the rust layer on carbon steel is related to the atmospheric corrosion rate of steel. In addition, another effect of cations was observed on the $Al^{3+}$ specimen which exhibited a relatively lower $E_{corr}$ due to the suppressed cathodic reaction, compared to the other specimens. As Evans *et al.* noted,[31] the anodic reaction (i.e., iron dissolution), is balanced with the cathodic reduction of $Fe^{3+}$ to $Fe^{2+}$ in rust layer. Therefore, the assumption that the $Al^{3+}$ incorporated in the rust layer prevented the reduction of $Fe^{3+}$ rationally supports the suppressed cathodic reaction in the initial stage of the cyclic corrosion test.

In the second stage, it is considered that the anodic reactions were further suppressed by the introduction of $Mg^{2+}$, $Al^{3+}$, $Cu^{2+}$ and $Ni^{2+}$ as $E_{corr}$ increased, accompanied by the decrease in $I_{corr}$. This is in accordance with previous works by Misawa *et al.* and Diaz *et al.*, who reported a suppressed anodic reaction by incorporated Ni in the rust layer.[32,33] One of the effects of the cations ($Mg^{2+}$, $Al^{3+}$, $Cu^{2+}$, and $Ni^{2+}$) might be the formation of a denser rust layer on the carbon steel, effectively retarding anodic dissolution.

### 4.2 Influence of α-FeOOH on the corrosion current density

As shown in Fig. 4, the composition of the rust layers formed on carbon steel was also affected by the additional immersion in the cation-containing solutions. Although β-FeOOH is likely to form in environments containing $Cl^-$ such as the solution used in the immersion stage of the cyclic corrosion test, α-FeOOH was preferentially formed on the specimens subjected to the additional immersion, especially on the $Al^{3+}$ and the $Ni^{2+}$ specimens. As the hydrolysis of metallic ions generates $H^+$, the additional immersion in the cation-containing solutions lowered the pH of the solution layer remaining on the specimen surface in the subsequent humid stage of the cyclic corrosion test. Consequently, α-FeOOH would be preferentially formed in such a slightly acidic environment, as pointed by Misawa.[34] Enhanced growth of α-FeOOH was also observed when Al was alloyed to a steel.[35,36] In addition, on the $Al^{3+}$ and the $Ni^{2+}$ specimens, the growth of β-FeOOH was clearly inhibited, which is also in accordance to previous works which reported that $Ni^{2+}$ excluded $Cl^-$ in the rust layer, thereby suppressing the formation of β-FeOOH.[23,33] Yamashita *et al.* found that not only the corrosion rate of weathering steels but also the composition of the rust formed on the steels changed during atmospheric corrosion.[15,37] Therefore, they introduced $\alpha/\gamma^*$ as an index of the protective ability of the rust layer,[10,16,38] where $\alpha$ and $\gamma^*$ indicate, respectively, the mass fraction of α-FeOOH and the total mass fractions of β-FeOOH, γ-FeOOH and $Fe_3O_4$.[16] $\alpha/\gamma^*$ was estimated from the mass fraction of the rust phases calculated from the area of the XRD peaks.

Figure 10 summarizes $I_{corr}$ with respect to the protective index, $\alpha/\gamma^*$ obtained for the rust layers formed after 3 cycles. $I_{corr}$ distinctly decreases with increasing $\alpha/\gamma^*$. In particular,

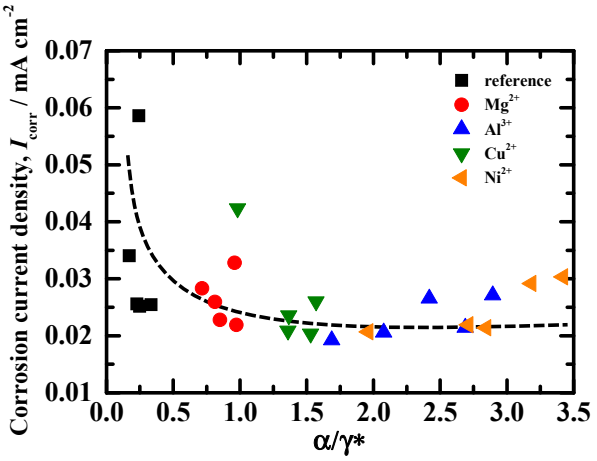


Fig. 10 Relation between corrosion current density and $\alpha/\gamma^*$.

$I_{corr}$ becomes less than approximately 0.03 mA/cm$^2$ when $\alpha/\gamma^*$ is more than 1. Therefore, the apparent correlation between $I_{corr}$ and $\alpha/\gamma^*$ implies that the corrosion of steel is fairly suppressed when the amount of α-FeOOH exceeds a critical threshold. This result is in good accordance with the previous work by Kamimura *et al.*[16] who reported that a weathering steel showed a low corrosion rate when $\alpha/\gamma^*$ was more than 1. Therefore, $\alpha/\gamma^*$ is the distinct index of the protectiveness of the rust layer formed in atmospheric corrosion environments.

The rust layer on the reference specimen contained a larger amount of $Fe_3O_4$, which was formed by the reduction of γ-FeOOH or β-FeOOH in the cyclic wet/dry process. However, the additional immersion in the cation-containing solutions suppressed the formation of $Fe_3O_4$. Keiser *et al.*[39] demonstrated that α-FeOOH was hard to be reduced electrochemically. Therefore, this low $I_{corr}$ observed at higher $\alpha/\gamma^*$ is attributed to the suppression of the cathodic reaction. If the cathodic process in atmospheric corrosion is mainly the reduction of corrosion products that cover the steel surface, the rust layer to be hardly reduced can suppress the anodic process.

The results of the present work demonstrated that the suppression of the cathodic reaction by additional immersion in cation-containing solutions effectively decreased $I_{corr}$, and that the addition of cations promoted the formation of fine α-FeOOH. The fine α-FeOOH is supposed to prevent the penetration of water, oxygen and aggressive corrosives such as $Cl^-$ which may enhance the dissolution of Fe. Thus, it can be inferred that the fine α-FeOOH in the rust layer suppressed both anodic and cathodic reactions. We can conclude that the modification of the rust layer on carbon steel by the introduction of cations to the rust will be an attractive approach to suppress the atmospheric corrosion of carbon steel.

## 5. Conclusion

In the present work, we proposed a simple approach to grow a protective rust layer on carbon steel during wet/dry cyclic atmospheric corrosion, that is, the introduction of cations in the rust layer by immersion in solutions containing

cations. Furthermore, the influence of the cations on the morphology, composition, and electrochemical properties of the rust layer on a carbon steel was examined. The following conclusions were drawn.

(1) XRD analyses indicated that the fraction of $\alpha$-FeOOH in the rust layers formed on the specimen subjected to the additional immersion in the cation-containing solutions, such as $Mg^{2+}$, $Cu^{2+}$, $Al^{3+}$, and $Ni^{2+}$ during the cyclic corrosion test, was larger than that of the reference specimen without the additional immersion.

(2) SEM observations of the rust layers formed after the cyclic corrosion test revealed that the additional immersion in the cation-containing solutions promoted the formation of dense rust layers on the carbon steel.

(3) The specimens subjected to the additional immersion in 1 M $CuSO_4$, $Al_2(SO_4)_3$, and $NiSO_4$ solutions exhibited a higher corrosion potential, $E_{corr}$, than the reference specimen, as $Cu^{2+}$, $Al^{3+}$, and $Ni^{2+}$ facilitated the formation of protective corrosion products. In addition, these specimens showed a lower $I_{corr}$. Thus, the cations improved the corrosion resistance.

(4) Correlation between $E_{corr}$ and $I_{corr}$ indicated that $Al^{3+}$ suppressed the cathodic reaction in the initial stage of the corrosion test. On the other hand, the anodic reaction was suppressed in the subsequent second stage by the cations.

(5) The additional immersion in the cation-containing solutions led to the formation of rust with smaller crystallite sizes, indicating that the cations in rust layer could suppress the growth of rust crystallites.

(6) $I_{corr}$ was less than 0.03 mA/cm$^2$ when the mass fraction of $\alpha/\gamma^*$ was more than 1. This suggested a high correlation between $I_{corr}$ and the composition of the rust layer formed on carbon steel.

## REFERENCES


1) F.U. Renner, A. Stierle, H. Dosch, D.M. Kolb, T.L. Lee and J. Zegenhagen: Nature **439** (2006) 707–710.
2) G.H. Koch, M.P.H. Brongers, N.G. Thompson, Y.P. Virmani and H. Payer: Corrosion Cost and Preventive Strategies in the United States, Report FHWA-RD-01-156, (Report by CC Technologies Laboratories, Inc. to Federal Highway Administration (FHWA), Office of Infrastructure Research and Development, McLean, 2001).
3) L. Hao, S.X. Zhan, J.H. Dong and W. Ke: Corros. Sci. **53** (2011) 4187–4192.
4) D. de la Fuente, I. Díaz, J. Simancas, B. Chico and M. Morcillo: Corros. Sci. **53** (2011) 604–617.
5) R. Cornell and U. Schwertmann: *The Iron Oxides, Structure, Properties, Reactions, Occurrences and Uses*, (VCH Publishers, Weinheim, Germany, 2003) pp. 1–38.
6) H. Tanaka, A. Miyafuji, K. Kandori, T. Ishikawa and T. Nakayama: Corros. Sci. **66** (2013) 337–342.
7) C. Rémazeilles and Ph. Refait: Corros. Sci. **49** (2007) 844–857.
8) M. Kimura, T. Suzuki, G. Shigesato, H. Kihara and S. Suzuki: ISIJ Int. **42** (2002) 1534–1540.
9) M. Morcillo, J.M. González-Calbet, J.A. Jiménez, I. Díaz, J. Alcántara, B. Chico, A. Mazarío-Fernández, A. Gómez-Herroro, I. Llorente and D. de la Fuente: Corrosion **71** (2015) 872–886.
10) S. Hara, T. Kamimura, H. Miyuki and M. Yamashita: Corros. Sci. **49** (2007) 1131–1142.
11) K. Asami and M. Kikuchi: Corros. Sci. **45** (2003) 2671–2688.
12) K. Kamimura, S. Nasu, T. Tazaki, K. Kuzushita and S. Morimoto: Mater. Trans. **43** (2002) 694–703.
13) M. Yamashita, K. Asami, T. Ishikawa, T. Ohtsuka, H. Tamura and T. Misawa: Zairyo-to-Kankyo **50** (2001) 521–530.
14) H. Okada, Y. Hosoi, K. Yukawa and H. Naito: Tetsu-to-Hagané **55** (1969) 355–365.
15) M. Yamashita, H. Miyuki, T. Matsuda, H. Nagano and T. Misawa: Corros. Sci. **36** (1994) 283–299.
16) T. Kamimura, S. Hara, H. Miyuki, M. Yamashita and H. Uchida: Corros. Sci. **48** (2006) 2799–2812.
17) SAE J2334, Cosmetic Corrosion Lab Test, SAE International, Warrendale, PA, (1998).
18) T. Kamimura, K. Kashima, K. Sagae, H. Miyuki and T. Kudo: Corros. Sci. **62** (2012) 34–41.
19) D.P. Schmidt, B.A. Shaw, E. Sikora, W.W. Shaw and L.H. Laliberte: Corrosion **63** (2007) 958–974.
20) S. Hara, M. Yamashita, T. Kamimura and M. Sato: J. Japan Inst. Metals **71** (2007) 346–353.
21) W.J. Chen, L. Hao, J.H. Dong and W. Ke: Corros. Sci. **83** (2014) 155–163.
22) I.M. Allam, J.S. Arlow and H. Saricimen: Corros. Sci. **32** (1991) 417–432.
23) T. Mizoguchi, Y. Ishii, T. Okada, M. Kimura and H. Kihara: Corros. Sci. **47** (2005) 2477–2491.
24) M. Kimura, H. Kihara, M. Nomura and Y. Kitajima: Corrosion in Marine and Saltwater Environments II-Proc. of the International Symposium; Symposium on Corrosion and Corrosion Control in Saltwater Environments II, (Electrochemical Society, 2005) pp. 133–142.
25) L. Hao, S. Zhang, J. Dong and W. Ke: Corros. Sci. **54** (2012) 244–250.
26) Y.Y. Chen, H.J. Tzeng, L.I. Wei, L.H. Wang, J.C. Oung and H.C. Shih: Corros. Sci. **47** (2005) 1001–1021.
27) K. Inouye, S. Ishii, K. Kaneko and T. Ishikawa: Z. Anorg. Allg. Chem. **391** (1972) 86–96.
28) K. Inouye, K. Ichimura, K. Kaneko and T. Ishikawa: Corros. Sci. **16** (1976) 507–517.
29) T. Nishimura, H. Katayama, K. Noda and T. Kodama: Corros. Sci. **42** (2000) 1611–1621.
30) M. Kimura and H. Kihara: Nippon Steel Technical Report **91** (2005) 86–90.
31) U.R. Evans and C.A.J. Taylor: Corros. Sci. **12** (1972) 227–246.
32) C. Wen, Y. Tian, G. Wang, J. Hu and P. Deng: Int. J. Electrochem. Sci. **11** (2016) 4161–4173.
33) X. Chen, J. Dong, E. Han and W. Ke: Mater. Lett. **61** (2007) 4050–4053.
34) T. Misawa: Corros. Sci. **13** (1973) 659–676.
35) T. Doi, K. Kitamura, K. Nakanishi, K. Kashima, T. Kamimura, H. Miyuki, T. Ohta and M. Yamashita: J. Japan Inst. Metals **74** (2010) 10–18.
36) T. Nishimura, A. Tahara and T. Kodama: Mater. Trans. **42** (2001) 478–483.
37) M. Yamashita, H. Miyuki, H. Nagano and T. Misawa: Zairyo-to-Kankyo **43** (1994) 26–32.
38) T. Kamimura, M. Yamashita, H. Uchida and H. Miyuki: J. Japan Inst. Metals **65** (2001) 922–928.
39) J.T. Keiser, C.W. Brown and R.H. Heidersbach: Corros. Sci. **23** (1983) 251–259.